Available online at www.sciencedirect.com
SCIENCE DIRECT®
Thin Solid Films 430 (2003) 125–129
thin solid films
www.elsevier.com/locate/tsf

# High-rate deposition of amorphous silicon films using hot-wire CVD with a coil-shaped filament

Henry S. Povolny*, Xunming Deng

*Department of Physics and Astronomy, University of Toledo, Toledo, OH 43606, USA*

**Abstract**

To reduce the manufacturing cost of amorphous silicon (a-Si:H)-based photovoltaic devices, it is important to deposit high-quality a-Si:H and related materials at a high deposition rate. To this end, we designed and constructed a hot-wire deposition chamber with a coiled filament design and with multiple gas inlets. The process gas could be directed into the chamber through the filament coil and have maximum exposure to the high-temperature filament surface. Using such a chamber design, we deposited a-Si:H films at high deposition rates up to 800 Å $s^{-1}$ and dense, low-void a-Si:H at rates up to 240 Å $s^{-1}$.


*Keywords:* Hot-wire deposition; Amorphous silicon; High deposition rate

## 1. Introduction

Considerable progress has been made in hydrogenated amorphous silicon (a-Si:H)-based thin film photovoltaic devices during recent years [1,2]. For high-efficiency solar cells, the a-Si:H layers in these devices have typically been deposited using RF plasma-enhanced chemical vapor deposition (PECVD). While RF PECVD produces cells with high efficiency, the deposition rates are generally low, approximately 1–5 Å $s^{-1}$. A number of alternative deposition techniques have been explored to deposit a-Si:H intrinsic layers at higher deposition rates. Using a very high frequency (VHF) PECVD process, high-efficiency solar cell devices have been produced with a-Si:H intrinsic layers deposited at approximately 10 Å $s^{-1}$ [3,4]. Hot-wire CVD (HWCVD) [5], also called the catalytic CVD (Cat-CVD) process [6], has been used to deposit a-Si:H based solar cells at higher deposition rates [7–9]. Although HWCVD-produced cells still show lower efficiency than those produced by PECVD, the potential to deposit a-Si:H at higher rates makes HWCVD an attractive process for a-Si:H solar cell fabrication. In addition to photovoltaic applications, a-Si:H is also used for other devices, such as charged particle detectors [10,11]. In these devices, p–i–n structures with i-layers of thickness up to 10–20 μm are used to detect alpha particles or neutrons. Therefore, it is important to explore deposition processes that can be used to deposit a-Si:H films at high deposition rates. In this paper we report our study on the high-rate deposition of a-Si:H films using a HWCVD process employing a coiled filament design [12] and high flow rates.

## 2. Chamber description

The hot-wire chemical vapor deposition (HWCVD) chamber, shown in Fig. 1, consists of a high vacuum chamber, a substrate holder, a coiled filament perpendicular to the substrate, two annular gas inlets near the substrate and one axial gas inlet directed through the filament coil, a gas confinement cup and an annular RF electrode for PECVD. The substrate holder, capable of holding a 10-cm×10-cm substrate, is inverted over the gas confinement cup. Deposition was made on a variety of substrates, including crystalline silicon (c-Si), quartz, 7059 glass, 1737 glass and stainless steel.

The filament coil is typically 1 m of 0.75-mm-diameter tungsten wire wound in a coil, approximately 7 mm in diameter and 5 cm long, with approximately 40 evenly spaced revolutions. Both 0.2- and 0.5-mm-diameter tungsten wires were tried, but did not support themselves at deposition temperatures. The filament is attached by a short, straight length of wire at the top

*Corresponding author.
*E-mail address:* hpovolny@physics.utoledo.edu (H.S. Povolny).

0040-6090/03/$ - see front matter 
doi:10.1016/S0040-6090(03)00090-7

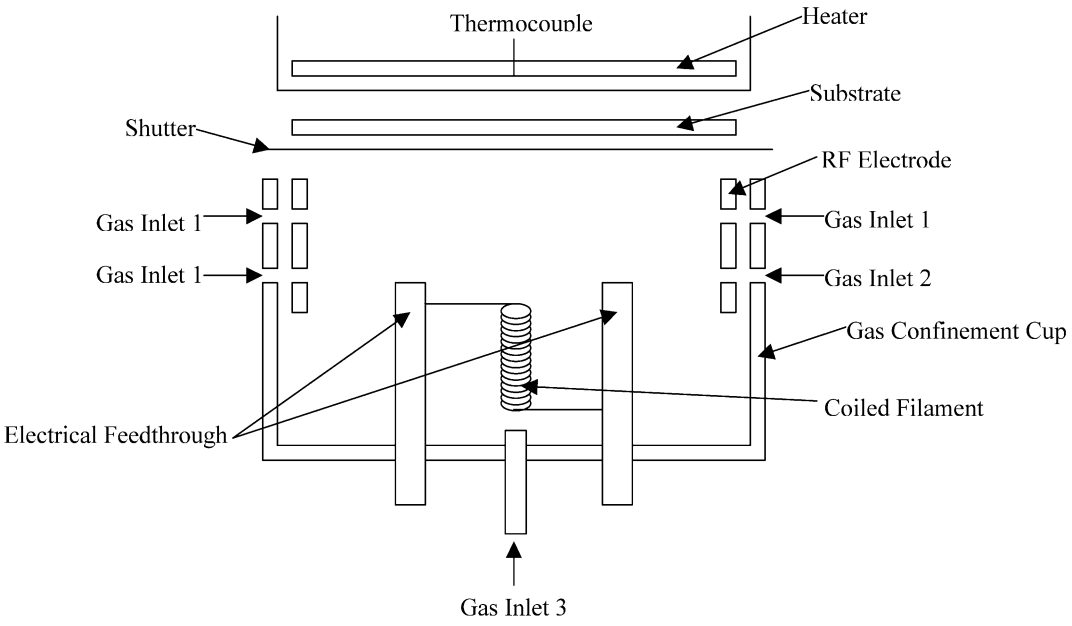


Fig. 1. Schematic diagram of the hot-wire CVD deposition chamber.

and bottom to two vertical posts running parallel to the filament on either side, approximately 2 cm away. The top of the filament can be positioned anywhere from 4.5 to 6.75 cm from the substrate, although 5.7 cm was the distance used for this study. The temperature of the filament was calibrated using an optical pyrometer in vacuum and with hydrogen flow at various pressures. To maintain the temperature of the 0.75-mm-diameter tungsten wire at 2000 °C, currents between 29.5 and 31.5 A were required, depending on gas flow. Only a slight dependence on flow rate was noted, although higher pressures sometimes required a current increase of 1–2 A to maintain filament temperature.

Process pressure ranged from 7 to 200 mTorr for HWCVD and 500 mTorr for PECVD. Process gas flows ranged from a few to 140 sccm. Deposition is fairly uniform over a 2-cm×2-cm area in the center of the substrate area, but falls off by 50% or less closer to the edge.

## 3. Experimental details

A series of nine samples was prepared at high flow rates, both with and without hydrogen dilution on a variety of substrates, including 1737 glass, 7059 glass, quartz, c-Si and stainless steel (SS). The pressure was 100 mTorr and the filament temperature $T_{fil}$ was 2000 °C for all samples. Mixtures of $Si_2H_6$ and $H_2$ were used as the process gases. The substrate temperature $T_{sub}$ ranged from 100 to 400 °C, which was the temperature (actually measured at the position of the heater) before filament was turned on. The actual temperature of the substrate is expected to be higher due to filament heating. The other deposition conditions are summarized

Table 1
Deposition conditions of a-Si:H films using HWCVD

| Sample | $Si_2H_6$ flow (sccm) | $H_2$ flow (sccm) | $T_{sub}$ (°C) | Time (s) | Thickness (μm) | Deposition rate (Å/s) | Sample ID |
|---|---|---|---|---|---|---|---|
| A1 | 105 | 0 | 100+ | 30 | 2.1 | 700 | HW107 |
| A2 | 105 | 0 | 200+ | 30 | 1.4 | 460 | HW113 |
| A3 | 105 | 0 | 300+ | 30 | 0.72 | 240 | HW112 |
| A4 | 105 | 0 | 400+ | 30 | 0.72 | 240 | HW111 |
| B2 | 105 | 100 | 200+ | 30 | 0.54 | 180 | HW108 |
| B3 | 105 | 100 | 300+ | 30 | 0.60 | 200 | HW109 |
| B4 | 105 | 100 | 400+ | 30 | 0.46 | 150 | HW110 |
| C | 70 | 0 | 175+ | 120 | 2.4 | 200 | HW105 |
| D | 140 | 0 | 100+ | 30 | 2.4 | 800 | HW106 |

All samples were deposited at 100 mTorr with a filament temperature of 2000 °C.

Table 2
Properties of a-Si:H films deposited using HWCVD

| Sample | $n$ | $E_g$ (opt) (eV) | $C_H$ (at.%) | $R^*$ | $\sigma_{dark}$ ($\Omega^{-1}$ cm$^{-1}$) | $\sigma_{photo}$ ($\Omega^{-1}$ cm$^{-1}$) | Photosensitivity |
|---|---|---|---|---|---|---|---|
| A1 | 1.9 | ~1.9 | >10 | 1.0 | $<2\times10^{-11}$ | $1\times10^{-10}$ | >5 |
| A2 | 2.3 | 1.74 | 12 | 0.90 | $<2\times10^{-11}$ | $2\times10^{-9}$ | $>1\times10^{2}$ |
| A3 | 3.6 | 1.63 | 10 | 0.17 | $4\times10^{-10}$ | $4\times10^{-9}$ | $9\times10^{0}$ |
| A4 | 3.7 | 1.61 | 6 | 0.11 | $4\times10^{-10}$ | $5\times10^{-9}$ | $1\times10^{1}$ |
| B2 | 3.6 | 1.78 | 19 | 0.50 | $<2\times10^{-11}$ | $2\times10^{-8}$ | $>1\times10^{3}$ |
| B3 | 3.9 | 1.62 | 7 | 0.04 | $3\times10^{-10}$ | $1\times10^{-8}$ | $4\times10^{1}$ |
| B4 | 4.3 | 1.63 | 3 | 0.05 | $2\times10^{-10}$ | $2\times10^{-8}$ | $1\times10^{2}$ |
| C | 3.6 | 1.63 | 8 | 0.36 | $2\times10^{-11}$ | $8\times10^{-8}$ | $4\times10^{3}$ |
| D | 1.6 | ~1.9 | >8 | 1.0 | $3\times10^{-11}$ | $6\times10^{-9}$ | $2\times10^{2}$ |

$R^*$ calculated using 2000 vs. 2100 cm$^{-1}$.

in Table 1. A surface profilometer was employed to measure film thickness. Transmission was measured to determine the thickness and refractive index from the interference fringes and bandgap from the Tauc plot. Fourier-transform infrared spectroscopy (FTIR) was performed to determine hydrogen content from the integrated area of the 640-cm$^{-1}$ peak and bond preference from comparing the 2000- (monohydride) and 2100-cm$^{-1}$ (dihydride) peak heights. The microstructure factor, $R^*$, the relative concentration of H in silicon dihydride and silicon polyhydride to the total H in the film, is calculated from the ratio of integrated absorption in the FTIR $[A_{2100}]/([A_{2100}]+[A_{2000}])$. Lower $R^*$ suggests that the film is dense and has fewer micro voids. Electrical conductivity was measured to determine dark conductivity ($\sigma_{dark}$), photoconductivity ($\sigma_{photo}$) and the photo/dark conductivity ratio.

## 4. Results

Table 1 shows the deposition conditions of a series of nine samples deposited under different conditions. Samples A1, A2, A3 and A4 were deposited at substrate temperatures of 100, 200, 300 and 400 °C, respectively. All of these four samples were deposited with a $Si_2H_6$ flow of 105 sccm without hydrogen dilution. Samples B2, B3 and B4 were deposited at $T_{sub}$ of 200, 300 and 400 °C, while the flow of $Si_2H_6$ and $H_2$ was kept at 105 and 100 sccm, respectively. Samples C and D were deposited with different $Si_2H_6$ flow, designed to determine whether the deposition rate is limited by $Si_2H_6$ gas flow. All of the nine samples were deposited at a pressure of 100 mTorr, filament temperature of 2000 °C and deposition time of 30 s, except sample C, which was deposited in 120 s. The deposition time was controlled by a shutter. The total time taken in opening and closing the shutter was estimated to be less than 1.5 s. The thickness reported in Table 1 was obtained using a surface profilometer, measured near the center of the film, directly above the coiled filament. From Table 1, it is evident that the deposition rate of the films ranges from 150 to 800 Å s$^{-1}$, depending on the $Si_2H_6$ gas flow and the substrate temperature.

The deposition uniformity is poor on the 10-cm×10-cm substrates due to the nature of the coiled filament and the fact that all of the process gases were directed into the chamber through the inlet adjacent to the filament. For example, profilometer measurements indicated that at a position 3 cm away from the center the film, thickness drops approximately 30%. However, the thickness is fairly uniform within a 2-cm×2-cm area near the center.

In Table 2, we summarize the results from UV-visible transmission spectroscopy, FTIR spectroscopy, and photo and dark conductivity measurements. The first column lists the refractive index $n$, calculated by dividing $nd$ from the transmission spectroscopy and $d$ from the profilometer measurement. We did not rely solely on the thickness obtained from transmission measurements, as there is a large variation in the refractive index in this set of films and the films may not be highly uniform in thickness. Here $n$ is the index in the long wavelength region. The optical bandgap $E_g$ was calculated using a Tauc plot $(\alpha h\nu)^{1/2}=B(h\nu-E_g)$. The bandgap for samples A1 and D is approximate, since the Tauc plots did not yield straight lines. The hydrogen content ($C_H$) was calculated from the bending mode of the Si–H absorption (640 cm$^{-1}$) in the FTIR spectrum. We use a conversion factor of $2.3\times10^{19}$ between H concentration and the integrated peak at 640 cm$^{-1}$ [5] and a Si density of $5\times10^{22}$ cm$^{-3}$ to calculate $C_H$. For samples A1 and D, the actual Si density could be lower, so the $C_H$ value could be higher than is listed in Table 2. The table also lists the film microstructure factor $R^*$, calculated from FTIR spectra. In the last three columns of Table 2, we show $\sigma_{dark}$, $\sigma_{photo}$, which was measured under unit sunlight intensity, and photosensitivity ($\sigma_{photo}/\sigma_{dark}$); $\sigma_{photo}$ and $\sigma_{dark}$ were measured using a coplanar geometry with painted silver paste electrodes.

For the four samples in series A that were deposited without H dilution, when $T_{sub}$ increases from 100 to 400 °C, the deposition rate $r_d$ drops from 700 to 240 Å $s^{-1}$, as observed from Table 1. However, as reflected in the increase in refractive index to ~3.7 and decrease in $R^*$, at higher $T_{sub}$, the films are dense with few micro voids. The bandgap drops from ~1.9 to 1.61 eV, due to the drop in $C_H$ in the film from 12 at.% or greater down to 6.0 at.% when $T_{sub}$ is increased from 100 to 400 °C, since at higher $T_{sub}$, more H diffuses out of the film during the deposition, leaving less H inside. $\sigma_{dark}$ increases with $T_{sub}$, consistent with the reduced bandgap at higher $T_{sub}$. $\sigma_{photo}$ increases with $T_{sub}$, partially due to the reduced bandgap and partially to the improved structural properties. There is no obvious trend in the photosensitivity, since $\sigma_{dark}$ is below the limit of the electrometer currently used in our set-up. Sample A1, although deposited at high deposition rate, contains a high concentration of H in dihydride and/or polyhydride forms, indicating a porous film, and is not of interest for photovoltaic applications.

With H dilution during the deposition, samples in series B show a similar trend, i.e. at higher $T_{sub}$ the films show higher $n$, lower bandgap and lower $C_H$, but with lower $R^*$. Comparing samples B2 and A2, a moderate level of H dilution, with $H_2/Si_2H_6 = 1{:}1.05$, reduces the deposition rate, but significantly improves the structural quality of the film, as reflected in the reduced $R^*$ and higher refractive index. B2 contains more H than A2 and has a slightly higher bandgap. Comparing samples B3 and B4 with A3 and A4, a moderate level of H dilution does not change the bandgap or $\sigma_{dark,}$ but it reduces $C_H$ and $R^*$, and increases $\sigma_{photo}$ and the photosensitivity, and is therefore beneficial.

Sample A1, A2, C and D exhibit the effect of $Si_2H_6$ gas flow $F$, as well as $T_{sub}$. At higher $F$ and lower $T_{sub}$ (samples A1 and D), the deposition rate is high, up to 800 Å $s^{-1}$. However, the film is porous, with $R^* = 1$. At higher $T_{sub}$ but lower $F$ (sample C), the film is denser and with low $R^*$, but with lower $r_d$, which is still much higher than the deposition rate typically reported in the literature, usually less than 50 Å $s^{-1}$. The photosensitivity is comparable among this set of films.

## 5. Discussion

We believe that the ability to grow films at high deposition rate is largely due to the highly efficient dissociation of gases at the filament due to the increased interaction time of the process gas with the filament. However, when the high flux of $SiH_3$ and other radicals arrive at the growth surface, $SiH_3$ radicals and H atoms do not have sufficient time to move around and find an appropriate site before the next radical arrives. Thus, the non-ideal structure gets 'frozen' and the material becomes porous. High temperature is needed so that the radicals on the surface can quickly move to favorable sites.

However, at these high temperatures, hydrogen diffuses out of the film at a correspondingly high rate. To maintain a high deposition rate and still retain H within the a-Si:H structure, we suggest rapid cooling of the substrate to below 250 °C after the completion of deposition at high $T_{sub}$. In this way, high surface mobility can be maintained during the growth to promote dense, void-free films, without losing hydrogen from the bulk due to effusion after the film is deposited.

## 6. Conclusion

Using a HWCVD process employing a coiled filament adjacent to the gas inlet, we deposited a-Si:H films at high deposition rates, in the range of 140–800 Å $s^{-1}$. The higher-rate samples are porous and contain H in mostly polyhydride bonding. At higher substrate temperature, a-Si:H films with low microstructure were deposited at a rate up to 240 Å $s^{-1}$. These films are dense, but with relatively low H content. We suggest that dense a-Si:H films could be deposited at a high rate (e.g. 800 Å $s^{-1}$) at a higher substrate temperature (e.g. 400 °C) but the substrates need to be rapidly cooled down from the growth temperature immediately after deposition to prevent H from effusing.

## Acknowledgments

The authors would like to thank W. Du, X.B. Liao, W. Wang and X. Yang for experimental assistance and A.H. Mahan for important discussions. This work was partially funded by the NREL Thin Film Partnership Program ZAF-8-17619-14 and NDJ-2-30630-08.

## References

[1] S. Guha, J. Yang, A. Banerjee, T. Glatfelter, K. Hoffman, S. Ovshinsky, M. Izu, H. Ovshinsky, X. Deng, Mater. Res. Soc. Symp. Proc. 336 (1994) 645.
[2] J. Yang, A. Banerjee, S. Guha, Appl. Phys. Lett. 70 (1997) 2977.
[3] A. Shah, J. Dutta, N. Wyrsch, K. Prasad, H. Curtins, F. Finger, A. Howling, C. Hollenstein, Mater. Res. Soc. Symp. Proc. 258 (1992) 15.
[4] X. Deng, S. Jones, T. Liu, M. Izu, S. Ovshinsky, Proceedings of the 26th Photovoltaic Specialists Conference, 1997, p. 591.
[5] A. Mahan, J. Carapella, B. Nelson, R. Crandall, I. Balberg, J. Appl. Phys. 69 (1991) 6728–6730.
[6] H. Matsumura, Jpn. J. Appl. Phys. 25 (1986) L949–951.
[7] A. Mahan, Y. Xu, B. Nelson, R. Crandall, J. Cohen, K. Palinginis, A. Gallagher, Appl. Phys. Lett. 78 (2001) 3788.

[8] Q. Wang, E. Iwaniczko, J. Yang, K. Lord, S. Guha, Mater. Res. Soc. Symp. Proc. 664 (2001) A7.5.1.
[9] S. Bauer, B. Schroeder, W. Herbst, M. Lill, Proceedings of the 2nd World Conference on Photovoltaic Solar Energy Conversion, 1998, p. 363.
[10] V. Perez-Mendez, J. Morel, S.N. Kaplan, R.A. Street, Nucl. Instrum. Methods Phys. Res. 252 (1986) 478.
[11] D. Holcomb, A. Wintenberg, X. Deng, Pixelated neutron beam monitor development, Proceedings of an International Workshop on Position-Sensitive Neutron Detectors—Status and Perspectives, June 2001, Hahn-Meitner-Institut, Berlin, Germany, 2001.
[12] M. Konagai, W. Kim, H. Tasaki, M. Hallerdt, K. Takahashi, AIP Conf. Proc. 157 (1987) 142–149.